Bioorganic Chemistry 112 (2021) 104957

Contents lists available at ScienceDirect

Bioorganic Chemistry

journal homepage: www.elsevier.com/locate/bioorg

Synthesis, *In-vitro* evaluation and molecular docking studies of oxoindolin phenylhydrazine carboxamides as potent and selective inhibitors of ectonucleoside triphosphate diphosphohydrolase (NTPDase)

Saira Afzal [a], Mariya al-Rashida [b], Abdul Hameed [a], Julie Pelletier [c], Jean Sévigny [c,d], Jamshed Iqbal [a,*]

[a] Centre for Advanced Drug Research, COMSATS University Islamabad, Abbottabad Campus, Abbottabad, Pakistan
[b] Department of Chemistry, Forman Christian College (A Chartered University), Lahore, Pakistan
[c] Centre de recherche du CHU de Québec, Université Laval, Québec City, QC, Canada
[d] Département de Microbiologie-Infectiologie et d'Immunologie, Faculté de Médecine, Université Laval, Québec City, QC, Canada

ARTICLE INFO

Keywords:
Oxoindolin
Carboxamide
Isatin
Molecular docking
Nucleoside triphosphate diphosphohydrolase inhibitors

ABSTRACT

Members of the ectonucleoside triphosphate diphosphohydrolases (NTPDases) constitute the major family of enzymes responsible for the maintenance of extracellular levels of nucleotides and nucleosides by catalyzing the hydrolysis of nucleoside triphosphate (NTP) and nucleoside diphosphates (NDP) to nucleoside monophosphate (NMP). Although, NTPDase inhibitors can act as potential drug candidates for the treatment of various diseases, there is lack of potent as well as selective inhibitors of NTPDases. The current study describes the synthesis of a number of carboxamide derivatives that were tested on recombinant human (*h*) NTPDases. The most promising inhibitors were **2h** (*h*-NTPDase1, IC_{50}: 0.12 ± 0.03 μM), **2d** (*h*-NTPDase2, IC_{50}: 0.15 ± 0.01 μM) and **2a** (*h*-NTPDase3, IC_{50}: 0.30 ± 0.04 μM; *h*-NTPDase8, IC_{50}: 0.16 ± 0.02 μM). Four compounds (**2e**, **2f**, **2g** and **2h)** were associated with the selective inhibition of *h*-NTPDase1 while **2b** was identified as a selective *h*-NTPDase3 inhibitor. Considering the importance of NTPDase3 in the regulation of insulin release, the NTPDase3 inhibitors were further investigated to elucidate their role in the insulin release. The obtained data suggested that compound **2a** was actively participating in regulating the insulin release without producing any effect on NTPDase3 mRNA. Moreover, the most potent inhibitors were docked within the active site of respective enzyme and the observed interactions were in compliance with *in vitro* results. Hence, these compounds can be used as pharmacological tool to further investigate the role of NTPDase3 coupled to insulin release.

1. Introduction

Adenosine triphosphate (ATP) is a versatile signalling molecule that is present in extracellular space and plays an important role in cell to cell communication [1–2]. Almost all the cells release ATP that in turn activates the purinergic receptors (P2X and P2Y receptors) and participates in different physiological functions such as hormone secretion, neurotransmission, sensory transmission, glial-neuron interaction and specific organ associated functions [3–5]. In pancreatic beta cells, ATP is co-released with insulin secretory granules and acts in an autocrine manner to regulate the insulin secretion. This regulation of insulin secretion is achieved by activating two subfamilies of cell membrane receptors: ligand gated ion channel (P2X) receptors and G-protein coupled (P2Y) receptors [6–9]. P2X receptors are ATP-gated ion channels which are subdivided into seven types (P2X1-7) and associated with the exchange of cation across the cell membrane [10–12]. Activation of P2X receptors by ATP induces an elevated intracellular Ca^{+2} that eventually leads to insulin secretion [8,13–14]. In contrast, P2Y receptors are coupled to G-protein and are comprised of eight members ($P2Y_{1,2,4,6,11,12,13,14}$). They signal through intracellular second messengers such as cyclic AMP (cAMP), inositol phosphate and Ca^{+2} [15–16]. Activation of P2Y receptors leads to an induction of inositol triphosphate coupled with the transient increase in intracellular Ca^{+2} level that ultimately results in insulin secretion. Hence, ATP operates through P2 receptor activation and amplifies the insulin secretion [9,17].

However, extracellular ATP is progressively metabolized by the

* Corresponding author.
E-mail address: drjamshed@cuiatd.edu.pk (J. Iqbal).

https://doi.org/10.1016/j.bioorg.2021.104957
Received 23 February 2021; Received in revised form 13 April 2021; Accepted 28 April 2021
Available online 30 April 2021

coordinated action of a network of ectoenzymes known as ecto-nucleotidases. This chain of ecto-nucleotidases is composed of four main enzyme families i.e. nucleotide pyrophosphatases/phosphodiesterases (NPPs), ectonucleoside triphosphate diphosphohydrolases (NTPDases), alkaline phosphatases (APs or ALPs), and ecto-5′-nucleotidase (e-5′-N) [18–22]. The ecto-nucleotidases catalyze the hydrolysis of nucleoside triphosphates, diphosphates, monophosphates and dinucleoside polyphosphate leading to formation of nucleoside diphosphate, nucleoside monophosphate, nucleoside, phosphate and inorganic pyrophosphate, respectively. Thus, these ecto-nucleotidases not only regulate the concentration of extracellular ATP and related nucleotides but also provide additional ligands for P2 and P1 receptors [3,23].

NTPDases is the principal enzyme family responsible for degradation of adenosine triphosphate and adenosine diphosphate (ADP). They are capable of hydrolyzing ATP to AMP (adenosine monophosphate) via ADP production [24–25]. So far, eight members (NTPDase1-8) of this family have been identified, each possessing distinct catalytic properties, substrate preference and tissue specific distribution [26–27]. Four members of this family (NTPDase1, −2, −3, −8) are ecto enzymes as their catalytic site is present in extracellular space [28–29] whereas, the remaining members have been designated as intracellular proteins and include NTPDase4, −5, −6 and −7 [27,30].

NTPDase3 is highly expressed in pancreatic β-cells where it has been described to regulate the insulin release [31,32]. Lavoie and co-workers used a commercially available non-selective NTPDase inhibitors termed as BG0136 and NF279. These studies revealed that the inhibition of NTPDase3 activity by BG0136 or NF279 affected insulin secretion [32]. Similarly, in another study treatment of pancreatic islets with ARL67156 (a non-selective NTPDase inhibitors) has been shown to induce insulin secretion [33]. Thus it can be suggested that blocking the ATP hydrolysis (by inhibiting NTPDase3) might represent a therapeutic strategy to treat type 2 diabetes. At present, there is lack of data addressing this particular role of NTPDase3 and only few studies have been undertaken to illustrate the involvement of NTPDase3 in insulin release. This scarcity of data encouraged us to synthesize a set of oxoindolin phenylhydrazine carboxamides that were likely to inhibit NTPDases. The sifted inhibitors (of NTPDase3) were proceeded towards the insulin secretion study.

2. Material and methods

All the chemicals and solvents were procured from commercial suppliers and were not subjected to any additional purification, unless specified otherwise. All reactions were checked by thin layer chromatography (TLC), performed on 200 μm thick aluminum sheets laminated with silica gel 60 F_{254} (Merck, Germany). Melting points were measured using a digital Gallenkamp melting point apparatus (UK) and were uncorrected. The IR spectra were determined using a Perkin Elmer BX-II spectrometer (USA). Mass spectra were obtained using an API 2000 mass spectrometer (Applied Biosystems, Germany). ^{1}H and ^{13}C spectra were recorded on a 300 MHz spectrophotometer (Bruker AM-300, USA) while using DMSO–d_6 as a solvent.

2.1. General procedure for the synthesis of substituted phenylhydrazine carboxamides (1a–j)

To a solution of hydrazine hydrate (in excess) in acetonitrile, corresponding isocyanates (1 mmol) were added drop wise. This reaction was carried out in an ice bath and allowed to stir for half an hour. The precipitated product was filtered off, washed and finally dried at room temperature.

2.2. General procedure for the synthesis of Oxoindolin-3-ylidene phenylhydrazine carboxamides (2a–j)

A solution consisting of isatin (1 mmol), an appropriate intermediate (**1a-j,** 1 mmol) and few drops of acetic acid was prepared in acetonitrile and then refluxed for 6–7 h. The precipitated solid was filtered, washed and dried.

2.2.1. N-(4-fluorophenyl)-2-(2-oxoindolin-3-ylidene)hydrazine-1-carboxamide (2a)

Yellow solid; Melting point = 223–225 °C; Yield: 79%; IR(KBr): 3349–3117(>NH stretch), 1701(>C═O), 1572(>C═N—), 1524(>NH bend), cm^{-1}; **^{1}HNMR** (300 MHz, DMSO-d_6): δ (ppm) 10.77 (s, 1H, NH), 10.43 (s, 1H, NH), 9.56 (s, 1H, NH), 8.08 (d, 1H, J = 7.8 Hz), 7.61 (dd, 2H, J = 9.0, 5.1 Hz), 7.38 (t, 1H, J = 7.8 Hz), 7.21–7.05 (m, 3H), 6.91 (d, 1H, J = 7.8 Hz); **^{13}C NMR** (75 MHz, DMSO-d_6) δ (ppm): 172.49, 165.17, 152.91, 143.60, 135.38, 132.45, 125.72, 122.07, 121.70, 121.60, 116.03, 115.73, 110.99 and positive mode m/z (%): 299 (97%)

2.2.2. N-(3-nitrophenyl)-2-(2-oxoindolin-3-ylidene)hydrazine-1-carboxamide (2b)

Yellow solid; Melting point = 225–228 °C; Yield: 74%; IR(KBr): 3343–3114(>NH stretch), 1694(>C═O), 1597(>C═N—), 1522(>NH bend), cm^{-1}; **^{1}H NMR** (300 MHz, DMSO-d_6): δ (ppm) 10.80 (s, 1H, NH), 10.57 (s, 1H, NH), 10.03 (s, 1H, NH), 8.64 (t, 1H, J = 2.1 Hz), 8.09 (d, 1H, J = 7.8 Hz), 7.99–7.90 (m, 2H), 7.63 (t, 1H, J = 8.1 Hz), 7.39 (td, 1H, J = 7.5, 0.75 Hz), 7.09 (t, 1H, J = 7.65 Hz), 6.92 (d, 1H, J = 7.8 Hz); **^{13}C NMR** (75 MHz, DMSO-d_6) δ (ppm): 165.07, 153.17, 148.53, 143.77, 140.45, 136.32, 132.70, 130.66, 125.92, 122.11, 117.91, 115.99, 113.88, 11.05 and positive mode m/z (%): 326 (97%)

2.2.3. N-(4-methoxyphenyl)-2-(2-oxoindolin-3-ylidene)hydrazine-1-carboxamide (2c)

Yellow solid; Melting point = 205–209 °C; Yield: 72%; IR(KBr): 3358–3218(>NH stretch), 1690(>C═O), 1589(>C═N—), 1511(>NH bend), cm^{-1}; **^{1}H NMR** (300 MHz, DMSO-d_6): δ (ppm) 10.77 (s, 1H, NH), 10.36 (s, 1H, NH), 9.34 (s, 1H, NH), 8.08 (d, 1H, J = 7.5 Hz), 7.51–7.46 (m, 2H), 7.37 (t, 1H, J = 7.65 Hz,), 7.08 (t, 1H, J = 7.35 Hz), 6.95–6.90 (m, 3H), 3.74 (s, 3H; Alkyl-H); **^{13}C NMR** (75 MHz, DMSO) δ (ppm): 172.52, 165.20, 155.68, 152.77, 143.49, 134.93, 132.12, 125.61, 122.05, 121.48, 116.09, 114.51, 110.96, 55.65 and positive mode m/z (%): 311 (69%)

2.2.4. N-(4-chlorophenyl)-2-(2-oxoindolin-3-ylidene)hydrazine-1-carboxamide (2d)

Yellow solid; Melting point = 215–217 °C; Yield: 74%; IR(KBr): 3345–3179(>NH stretch), 1690(>C═O), 1595(>C═N—), 1537(>NH bend), cm^{-1}; **^{1}H NMR** (300 MHz, DMSO-d_6): δ (ppm) 10.78 (s, 1H, NH), 10.44 (s, 1H, NH), 9.65 (s, 1H, NH), 8.08 (d, 1H, J = 7.5 Hz), 7.65–7.60 (m, 2H), 7.39 (m, 3H), 7.08 (t, 1H, J = 7.5 Hz), 6.91 (d, 1H, J = 7.5 Hz); **^{13}C NMR** (75 MHz, DMSO-d_6) δ (ppm): 165.15, 152.75, 143.64, 138.05, 135.65, 132.52, 129.20, 127.06, 125.75, 122.08, 121.27, 116.02, 111.02 and positive mode m/z (%): 315 (99%)

2.2.5. N-(2,6-dimethylphenyl)-2-(2-oxoindolin-3-ylidene)hydrazine-1-carboxamide (2e)

Yellow solid; Melting point = 186–189 °C; Yield: 75%; IR(KBr): 3355–3274(>NH stretch), 1703(>C═O), 1580(>C═N—), 1520(>NH bend), cm^{-1}; **^{1}H NMR** (300 MHz, DMSO-d_6): δ (ppm) 10.77 (s, 1H, NH), 10.50 (s, 1H, NH), 10.34 (s, 1H, NH), 8.09 (t, 1H, J = 10.0 Hz), 7.37 (t, 1H, J = 7.65 Hz), 7.12–7.04 (m, 4H), 6.91 (d, 1H, J = 7.8 Hz), 2.19 (d, 6H, J = 9.6 Hz, Alkyl-H); **^{13}C NMR** (75 MHz, DMSO) δ (ppm): 167.11, 153.16, 143.15, 136.21, 133.12, 132.51, 130.12, 128.27, 127.82, 122.63, 121.74, 115.45,18.62 and positive mode m/z (%): 309 (98%)

2.2.6. N-(2,6-dichlorophenyl)-2-(2-oxoindolin-3-ylidene)hydrazine-1-carboxamide (2f)

Yellow solid; Melting point = 198–200 °C; Yield: 70%; IR(KBr): 3345–3205(>NH stretch), 1694(>C═O), 1595(>C═N—), 1530(>NH bend), cm^{-1}; **^{1}H NMR** (300 MHz, DMSO-d_6): δ (ppm) 10.77 (s, 1H, NH), 10.35 (s, 1H, NH), 9.09 (s, 1H, NH), 8.03 (d, 1H, J = 7.5 Hz), 7.51 (d, 2H,

$J = 8.1$ Hz), 7.40–7.27 (m, 2H), 7.06 (t, 1H, $J = 7.5$ Hz), 6.91 (d, 1H, $J = 7.8$ Hz); **^{13}C NMR** (75 MHz, DMSO-d_6) δ (ppm): 166.15, 152.20, 145.13, 138.32, 136.12, 133.01, 130.24, 128.87, 127.24, 122.90, 121.14, 120.50, 115.92 and positive mode *m/z* (%): 350 (88%)

2.2.7. N-(2,4-dimethoxyphenyl)-2-(2-oxoindolin-3-ylidene)hydrazine-1-carboxamide (2g)

Yellow solid; Melting point = 200–203 °C; Yield: 75%; IR(KBr): 3367–3022(>NH stretch), 1692(>C═O), 1604(>C═N—), 1533(>NH bend), cm^{-1}; **^{1}H NMR** (300 MHz, DMSO-d_6): δ (ppm) 10.78 (s, 2H, NH), 9.02 (s, 1H, NH), 8.17 (d, 1H, $J = 7.8$ Hz), 7.95 (d, 1H, $J = 8.7$ Hz,), 7.36 (t, 1H, $J = 7.5$ Hz), 7.06 (t, 1H, $J = 7.65$ Hz), 6.90 (d, 1H, $J = 7.5$ Hz), 6.67 (d, 1H, $J = 2.4$ Hz), 6.54 (dd, 1H, $J = 8.85$, 2.55 Hz), 3.88 (s, 3H; Alkyl-H), 3.75 (s, 3H, Alkyl-H); **^{13}C NMR** (75 MHz, DMSO) δ (ppm): 172.53, 165.14, 156.36, 152.62, 150.35, 143.61, 134.51, 132.33, 125.81, 122.00, 120.87, 116.01, 110.90, 104.73, 99.28, 56.39, 55.78 and positive mode *m/z* (%): 341 (89%)

2.2.8. N-(4-nitrophenyl)-2-(2-oxoindolin-3-ylidene)hydrazine-1-carboxamide (2h)

Yellow solid; Melting point = 255–257 °C; Yield: 80%; IR(KBr): 3328–3175(>NH stretch), 1697(>C═O), 1593(>C═N—), 1526(>NH bend), cm^{-1}; **^{1}H NMR** (300 MHz, DMSO-d_6): δ (ppm) 10.82 (s, 1H, NH), 10.57 (s, 1H, NH), 110.20 (s, 1H, NH), 8.25 (d, 2H, $J = 9.0$ Hz,), 8.08 (d, 1H, $J = 7.5$ Hz), 7.85 (d, 2H, $J = 9.3$ Hz), 7.40 (t, 1H, $J = 7.8$ Hz), 7.10 (t, 1H, $J = 7.65$ Hz), 6.92 (d, 1H, $J = 7.8$ Hz,); **^{13}C NMR** (75 MHz, DMSO-d_6) δ (ppm): 165.07, 152.64, 145.66, 143.83, 142.36, 136.66, 132.79, 125. 92, 123.57, 122.12, 119.09, 115.92, 111.10 and positive mode *m/z* (%): 326 (96%)

2.2.9. 2-(2-oxoindolin-3-ylidene)-N-(3-(trifluoromethyl)phenyl) hydrazine-1-carboxamide (2i)

Yellow solid; Melting point = 157–160 °C; Yield: 76%; IR(KBr): 3324–3218(>NH stretch), 1688(>C═O), 1600(>C═N—), 1537(>NH bend), cm^{-1}; **^{1}HNMR** (300 MHz, DMSO-d_6): δ (ppm) 11.06 (s, 1H, NH), 9.66 (s, 1H, NH), 9.35 (s, 1H, NH), 7.62–7.49 (m, 4H), 7.32 (d, 1H, $J = 7.8$ Hz), 7.06 (t, 1H, $J = 7.5$ Hz), 6.91 (d, 1H, $J = 7.8$ Hz); **^{13}C NMR** (75 MHz, DMSO-d_6) δ (ppm): 184.87, 182.74, 159.83, 153.10, 151.17, 143.81, 142.24, 140.85, 138.82, 130.43, 125.15, 123.21, 122.34, 118.51, 114.55, 112.65 and positive mode *m/z* (%): 349 (96%)

2.2.10. N-benzyl-2-(2-oxoindolin-3-ylidene)hydrazine-1-carboxamide (2j)

Yellow solid; Melting point = 193–196 °C; Yield: 83%; IR(KBr): 3350–3125(>NH stretch), 1682(>C═O), 1599(>C═N—), 1526(>NH bend), cm^{-1}; **^{1}H NMR** (300 MHz, DMSO-d_6): δ (ppm) 11.99 (s, 1H, NH), 10.72 (s, 1H, NH), 10.35 (s, 1H, NH), 8.06 (d, 1H, $J = 7.5$ Hz), 7.80 (t, 1H, $J = 6$ Hz), 7.36–7.23 (m, 5H), 7.02 (t, 1H, $J = 7.35$ Hz), 6.88 (d, 1H, $J = 7.5$ Hz), 4.41 (d, 2H, $J = 6$ Hz, CH_2); **^{13}C NMR** (75 MHz, DMSO-d_6) δ (ppm): 172.53, 165.16, 155.54, 143.38, 140.26, 134.14, 132.15, 128.77, 127.79, 125.73, 122.03, 116.10, 110.81, 43.36 and positive mode *m/z* (%): 295 (95%)

2.3. Biological protocols

2.3.1. Enzyme preparations of NTPDases

Recombinant *h*-NTPDases were expressed by transfecting the COS-7 cells in 15 cm dishes using Lipofectamine as transfection reagent as previously described [34–35]. In short, confluent cells were incubated in Dulbecco's Modified Eagle's Medium (serum free) along with plasmid (6 μg) and Lipofectamine (24 μL) at 37 °C (5 h). Following the termination of transfection, cells were collected by harvesting 40–72 h later.

Subsequently, the transfected cells were washed with tris-saline buffer (at 4 °C) and used to prepare the protein extracts. Afterwards, the cells were harvested by scrapping and transferred to harvesting medium comprised of NaCl (95 mM), tris (45 mM) and phenylmethylsulfonyl fluoride (0.1 mM), pH 7.5 and passed through another washing by centrifugation (300 × g, 4 °C) for 5 min. The washed cells were resuspended in harvesting buffer incorporating aprotinin (10 μg/mL) and then sonicated. Finally, nuclei and cellular debris were discarded by another centrifugation (300 × g, 4 °C, 10 min) and resulting protein extracts were aliquoted and stored at −80 °C. Protein concentration of these protein extracts was estimated by Bradford microplate assay while using bovine serum albumin as a standard [36].

2.3.2. NTPDase activity assay

NTPDase activity was assayed using malachite green reagent as previously described, with slight modifications [37]. The assay was performed in 50 mM tris HCl buffer (pH 7.4) containing 5 mM $CaCl_2$. Solutions of synthesized products were prepared in 10% DMSO solution and were tested at 100 μM concentration. Firstly, assay buffer (55 μL) and test compound solution (10 μL) were incubated with 10 μL of enzyme solution for 10 min at 37 °C. The concentration of enzyme (per well) used was as follows; *h*-NTPDase1 (59 ng), *h*-NTPDase2 (43 ng), *h*-NTPDase3 (105 ng), *h*-NTPDase8 (89 ng). The reaction was started by adding 10 μL of substrate solution (i.e. ATP) with a final concentration of 100 μM. Then, the reaction was again incubated at 37 °C for 15 min. Finally, malachite green reagent (15 μL) was added to terminate the reaction and a room temperature incubation was carried out. After 4–6 min, the absorbance of reaction mixture was measured on Omega FLUOstar microplate reader (BMG Labtech, Germany) using a wavelength of 630 nm. Percent inhibitions were computed for each compound and all those compounds exhibiting > 50% inhibition of any enzyme were further diluted to determine the IC_{50} values. Three independent inhibition experiments were conducted in triplicate, dose response curves were fitted and IC_{50} values were calculated using PRISM 5.0 (GraphPad, San Diego, USA).

2.3.3. Islets isolation

In this study, BALB/c mice (30–40 g in weight) were used at 6–8 weeks of age to isolate the pancreatic islets. The animals were kept in an environmentally controlled room at a temperature of 25 ± 2 °C with a 12-h light/12-h dark cycle. All procedures involving animal surgery were in compliance with internationally accepted protocols. In addition, all the protocols were approved by institutional committee on animal care and use. (Protocol: PHM.Eth./CS-M01-020-1609)

Isolation of mice islets was performed according to previously described protocol [38]. Following a general anesthesia, mice were killed by cervical dislocation and placed under dissection microscope. After identifying the ampulla, it was clamped and pancreas was distended with collagenase solution (3 mL), prepared at a concentration of 1 mg/mL. The distended pancreas was excised from the underlying connective tissue, placed in a 50 mL tube containing collagenase solution and digested at 37 °C for 15 min. In order to stop the digestion, tube was placed on ice and 20 mL of HBSS was added to wash the digested islets by centrifugation at 4 °C for 1 min at 1000 rpm. This washing was performed for 2–3 times and then islets were strained through a cell strainer (70 μm). Finally, the islets were hand-picked under microscope. All the steps involving isolation and purification of islets were performed in HBSS, in the absence of calcium, magnesium and phenol red.

2.3.4. Insulin secretion by isolated islets

Isolated islets were maintained in Krebs-Ringer bicarbonate buffer (KRBB, pH 7.4) that was comprised of 118 mM NaCl, 1.9 mM $CaCl_2$, 4.7 mM KCl, 25 mM $NaHCO_3$, 1.2 mM $MgSO_4$, 10 mM HEPES and 0.1% bovine serum albumin. During pre-incubation, islets (3 islets/vial) were suspended in KRBB containing low glucose concentration (3 mM) at 37 °C for 45 min. Then, KRBB was substituted with fresh media supplemented with high glucose concentration (16.7 mM) and islets were exposed to test compounds for 1 h at 37 °C. Following incubation, supernatant of each sample was removed and an aliquot of this sample was diluted to determine the amount of secreted insulin. The insulin secretion was quantified using mouse specific insulin ELIZA kit obtained from

Crystal Chem Inc. (USA), in compliance with manufacturer's directions. The optical density was recorded at a wavelength of 450 nm and the amount of insulin release was normalized to number of islets [38].

2.3.5. Ectonucleotidase activity of islets

2.3.5.1. Islets' homogenate preparation. Freshly isolated islets were transformed into a homogenate in compliance with a previously described procedure [39]. Briefly, islets after washing with HBSS were added to an ice-cold buffer composed of 0.25 M sucrose, 1 mM EDTA and 5 mM tris-HCl, pH 7.0. As a result, a suspension was formed and an appropriate amount of tris buffer (pH 7.4) was added to dilute it. The suspension was then sonicated for 30 *sec* resulting in the preparation of a homogenate. Finally, nucleus and cellular debris was separated by a centrifugation (15,000 rpm, 4 °C, 10 min) and supernatant was removed and kept at −20 °C till used in activity experiments. Bradford method was used to estimate the protein concentration while using bovine serum albumin as reference standard [36].

2.3.5.2. Ectonucleotidase activity of islet homogenate. After preparing the islet homogenate, the ectonucleotidase activity was determined by quantifying the liberated Pi using a colorimetric assay where KH_2PO_4 was utilized as a standard [32]. In order to derive a standard curve, KH_2PO_4 was diluted and incubated with malachite green reagent at room temperature. At the end, absorbance was recorded at 630 nm and plotted against concentrations to construct a standard curve.

The reaction medium was comprised of tris-HCl (50 mM, pH = 7.4) supplemented with 5 mM $CaCl_2$. The synthesized molecules were screened at 100 μM concentrations and the working solution of these inhibitors were formulated in 10% DMSO. Tris buffer (56 μL) containing test compound (10 μL) was incubated with 6 μL of islet homogenate (containing 6 μg of protein) at 37 °C. Following a 10 min incubation, reaction was initiated by adding 10 μL of ATP (100 μM) and incubated for 15 min at 37 °C. Afterwards, an aliquot of trichloroacetic acid (10%, 100 μL) was introduced to terminate the reaction followed by an incubation (15 min.) of samples on ice. At the end, each sample was mixed with an appropriate quantity of malachite green reagent and liberated inorganic phosphate (Pi) was measured using standard curve. In order to generate the dose response curve, each compound was tested at different concentrations. Ectonucleotidase activity was described in the form of nm of Pi/min/mg of protein. All the experiments were performed in triplicate.

2.3.6. Real time qPCR

2.3.6.1. Incubation of islets with test compounds. After washing the isolated islets, they were maintained at 37 °C for 45 min in KRB buffer containing low glucose concentration (3 mM). The islets were then exposed to test compounds for 3 h (37 °C) whereas, KRBB (supplemented with 16.7 mM glucose) was used as incubation medium. At the end, supernatant was separated while islets were used to extract the RNA.

2.3.6.2. RNA extraction and real time qPCR. Total RNA extraction from mice islets was carried out using the TRIzol reagent, following the manufacturer's instructions. After quantifying the RNA, cDNA was generated by reverse transcribing 1 μg of this RNA. Briefly, a reaction mixture (12 μL) composed of 1 μg RNA and 20 μM oligo-dT (1 μL) was prepared, incubated for 5 min. at 65 °C and instantly placed on ice. Then, an 8 μL aliquot of master mix consisting of buffer (5X, 4 μL), dNTPs mix (10 mM, 2 μL), RNase inhibitor (1 μL) and reverse transcriptase (1 μL) was added to above mentioned reaction mixture. The resulting sample was mixed by gentle pipetting and run under following temperature profile: 5 min at 25 °C, 70 min at 42 °C and 5 min at 70 °C. One microliter of cDNA was used for PCR in a total volume of 20 μL. Hence, PCR reaction mixture consisting of cDNA (1 μL), forward and revers primers (0.25 μL each) and SYBR Green master mix (10 μL) was formulated and PCR protocol was set as follows: one cycle of 95 °C for 10 min followed by 40 cycles of 95 °C for 15 *sec* and 55 °C for 60 *sec*. Reactions were carried out with PikoReal 96 Real-Time PCR system (Thermo Scientific, Vantaa, Finland). PCR of β actin was carried out as a control for cDNA synthesis and relative expression levels were determined using $\Delta\Delta C_T$ method.

2.4. Molecular docking studies

The protein data bank does not contain the crystal structures of human NTPDases, therefore, their homology models were built in accordance with our previously described procedure [40]. MOE was used for the preparation and energy minimization of selected compounds whereas, structures of enzymes were prepared using the BioSolveIT's LeadIT software [41]. Finally, docking studies were carried out with the help of BioSolveIT's LeadIT software and the most favorable pose with highest affinity and lowest binding energy was selected to study the binding interactions.

2.5. Statistical analysis

Data was shown as mean ± S.E.M. One-way ANOVA and student *t* test were performed by the PRISM 5.0 software.

3. Results and discussion

3.1. Chemistry

A series of 10 oxoindolin phenylhydrazine carboxamide derivatives (**2a-j**) was synthesized as potential inhibitors of NTPDases. It started with the synthesis of substituted phenylhydrazine carboxamide (**1a**–**j**) (Scheme 1).

The synthesized derivatives were exploited as starting material for the synthesis of target compounds and refluxed with isatin for 5–6 h (Table 1). Finally, precipitates of target compounds were obtained by evaporating the solvent at room temperature. The obtained precipitates were filtered, washed and characterized using IR, ^{1}H NMR and ^{13}C NMR and LC/ESI-MS.

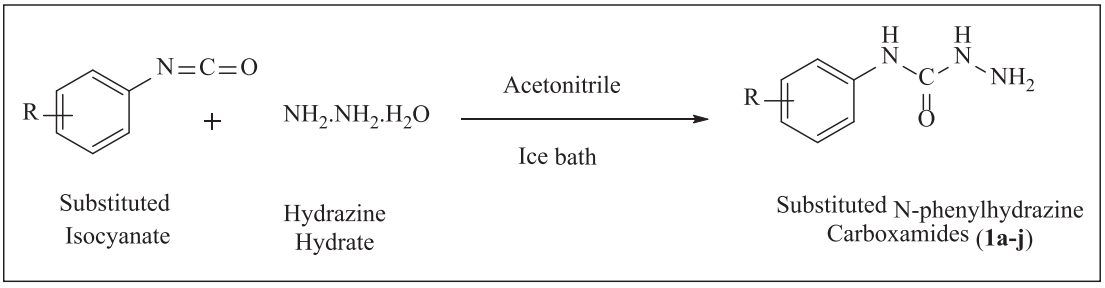

Scheme 1. Synthesis of substituted *N*-phenylhydrazine carboxamides (**1a–j**).

Table 1
Synthesis of target compounds **(2a–j)**.

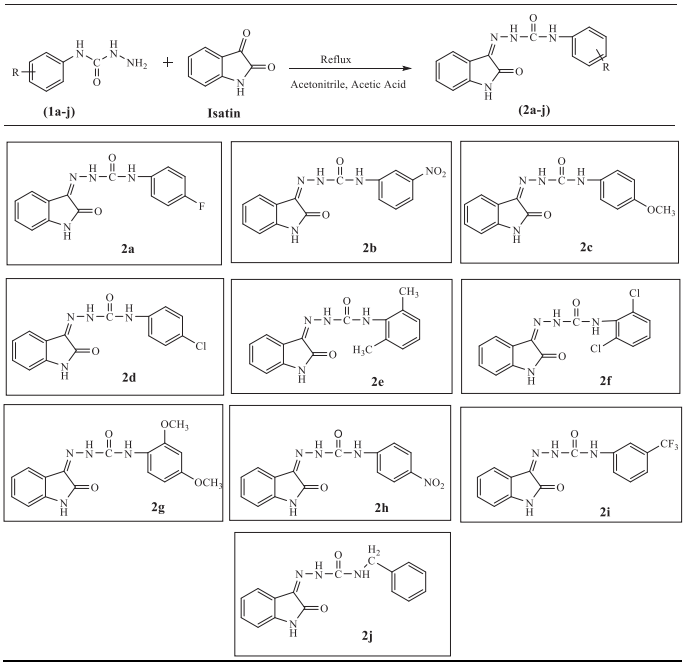

The identity of these products was established by IR, ^{1}H NMR, ^{13}C and mass spectra. Several peaks indicating the presence of specific functional groups were observed in IR spectra of these molecules. In this regard, absorption bands observed within the range of 3367–3302 cm^{-1} were corresponding to the NH stretching of amide and indole group. The peaks for C═O and C═N were observed in the region of 1703–1682 (cm^{-1}) and 1604–1572 (cm^{-1}), respectively. Similarly, the peaks in the region of 1537–1511 (cm^{-1}) were due to the presence of N—H. The ^{1}H NMR spectra of the compounds showed three characteristic singlets in the region of δ (ppm) 9.02–10.35, 9.02–10.72, and 10.77–11.99, which appeared due to CO—NH, NH of indole and —N—NH, respectively. Presence of these three —NH peaks clearly indicated the formation of target molecules. As per our anticipation, aromatic protons showed their signals in the range of δ (ppm) 8.64–6.54. The ^{13}C spectra revealed carbonyl peaks in the range of δ (ppm) 184.87–165.07, while amide and imine carbon signals were observed in the range δ (ppm) 182.74–152.20 and 159.83–143.15, respectively. Mass spectra of these compounds were obtained (in positive mode) and molecular ion peak for each compound was observed at respective *m/z*.

3.2. Inhibitory activity of compounds on recombinant h-NTPDases

This series of carboxamides (**2a–j**) was evaluated to determine inhibitory activity of these molecules against *h*-NTPDases. Four recombinant isozymes (*h*-NTPDase1, −2, −3 and −8) were used and test compounds were screened at an initial concentration of 0.1 mM. The results are presented in Table 2.

3.2.1. Structure activity relationships

It was observed that *h*-NTPDase1 was the most receptive enzyme and activity of many compounds was in micro molar range against *h*-NTPDase1. Interestingly, four compounds (**2e**, **2f**, **2g**, **2h**) were inhibiting the *h*-NTPDase1 selectively, having micro-molar IC_{50} values. However, these compounds affected other isozymes to a lesser extent.

Except **2b**, **2c** and **2j**, all the compounds inhibited *h*-NTPDase1 (>50%) and their dose response curves were generated. Among them, IC_{50}s of five compounds were < 1 μM and they included **2h**, **2d**, **2i**, **2a** and **2f**. From a structure–activity viewpoint, it was observed that *h*-NTPDase1 inhibitory activity was strongly enhanced by introducing electron withdrawing moiety (F, Cl, CF_3 and NO_2) at phenyl ring as compared to electron donating moiety (CH_3, OCH_3). It can be

Table 2
NTPDase Inhibitory Activity of Compounds **(2a–j)**.

Code	*h*-NTPDase1	*h*-NTPDase2	*h*-NTPDase3	*h*-NTPDase8
	IC_{50} (μM)[a] ± SEM/%inhibition[b]			
2a	0.37 ± 0.02 [a]	0.27 ± 0.02[a]	0.30 ± 0.04[a]	0.16 ± 0.02[a]
2b	45.9 ± 1.31[b]	44.8 ± 0.93[b]	2.82 ± 0.10[a]	42.2 ± 0.46[b]
2c	47.5 ± 0.58[b]	27.1 ± 0.71[b]	48.8 ± 0.87[b]	36.4 ± 0.38[b]
2d	0.16 ± 0.01[a]	0.15 ± 0.01[a]	40.0 ± 0.59[b]	45.7 ± 1.22[b]
2e	2.30 ± 0.04[a]	25.8 ± 1.34[b]	32.4 ± 1.18[b]	37.1 ± 0.48[b]
2f	0.70 ± 0.01[a]	32.1 ± 0.66[b]	41.1 ± 2.21[b]	27.9 ± 0.75[b]
2g	1.09 ± 0.05[a]	35.0 ± 2.41[b]	29.3 ± 0.49[b]	24.7 ± 1.31[b]
2h	0.12 ± 0.03[a]	41.1 ± 1.52[b]	27.5 ± 1.5[b]	27.6 ± 0.87[b]
2i	0.29 ± 0.01[a]	30.9 ± 0.62[b]	1.46 ± 0.08 [a]	28.7 ± 0.39[b]
2j	45.2 ± 1.27[b]	42.1 ± 0.98[b]	20.5 ± 1.14[b]	41.4 ± 1.50[b]
Suramin	16.1 ± 1.02[a]	24.1 ± 3.01[a]	4.31 ± 0.41[a]	101.1 ± 2.34[a]

[a] IC_{50} values are presented as mean ± SEM of three independent experiments.
[b] Percent inhibition determined at 100 μM.

exemplified by making a comparison of **2e** with **2f**. Similarly, a comparison between **2c** and **2d** also makes the electron withdrawing group more favorable

Likewise, the most active inhibitor against *h*-NTPDase1 (**2h**, IC_{50} = 0.12 ± 0.03 μM) also incorporated NO_2 substituted phenyl ring which is an electron withdrawing group. However, this activity seemed to be position dependent because incorporating the same NO_2 group at *meta* position resulted in <50% inhibition. It seems that activity due to NO_2 group is also position dependent.

Another trend observed here was the number of substitution and it was observed that compounds mono substituted with electron withdrawing scaffold were more active than those of di substituted. For instance, **2d** (containing 4-Cl phenyl ring) was 4 times more potent than **2f** (possessing 2,6-dichloro phenyl ring) in terms of IC_{50} value.

In case of *h*-NTPDase2, only two compounds (**2a** and **2d**) were recognized as potent inhibitors as indicated by their IC_{50} values (<1 μM). Structures of both the compounds possessed a F- or Cl-substituted phenyl ring, thus implying the importance of electron withdrawing group. Moreover, compound **2d** showed a dual inhibitory profile against *h*-NTPDase1 and *h*-NTPDase2 sharing almost an equal IC_{50} value. However, rest of the compounds showed < 50% inhibition of *h*-NTPDase2.

Moving towards next isozyme, three compounds appeared to be potential *h*-NTPDase3 inhibitors with their IC_{50}s ranging between 0.30 ± 0.04 μM to 2.82 ± 0.10 μM. Compound **2a** was the most active *h*-NTPDase3 inhibitor (IC_{50} = 0.30 ± 0.04 μM) whereas, IC_{50} of compound **2b** and **2i** was 2.82 ± 0.10 μM and 1.46 ± 0.08 μM, respectively. Here compound **2b** emerged as an important compound since it selectively inhibited the *h*-NTPDase3.

Except compound **2a**, all the compounds exhibited < 50% inhibition of *h*-NTPDase8. Thus, this isoform was least affected by these compounds.

3.2.2. *Enzyme kinetics studies of carboxamide derivatives*

Kinetic studies were performed for compounds **2h** and **2d** as the most active inhibitors of *h*-NTPDase1 and *h*-NTPDase2. Since compound **2a** showed the dual inhibition of *h*-NTPDase3 and *h*-NTPDase8, it was selected to perform kinetics studies against both enzymes. Hence mechanism of action was demonstrated by generating Lineweaver Burk plot for each compound. It was observed that compound **2h** was an uncompetitive inhibitor of *h*-NTPDase1 (Fig. 1) whereas, **2d** inhibited the *h*-NTPDase2 competitively (Fig. 2). Likewise, compound **2a** was also a competitive inhibitor of *h*-NTPDase3 and *h*-NTPDase8 (Figs. 3, 4).

3.3. *Effect of NTPDase3 inhibitors on insulin secretion*

In order to determine the effects of NTPDase3 inhibitors on insulin secretion, compound **2a**, **2b** and **2j** were incubated with mice pancreatic

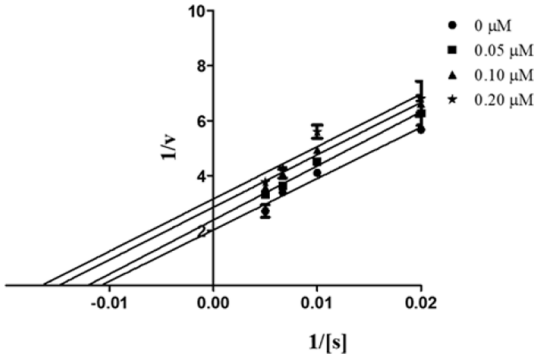

Fig. 1. Mode of inhibition of *h*-NTPDase1 inhibitor (**2h**) indicated by Lineweaver-Burk Plot. Inhibitor (**2h**) was used at following concentrations (μM): 0, 0.05, 0.10 and 0.20.

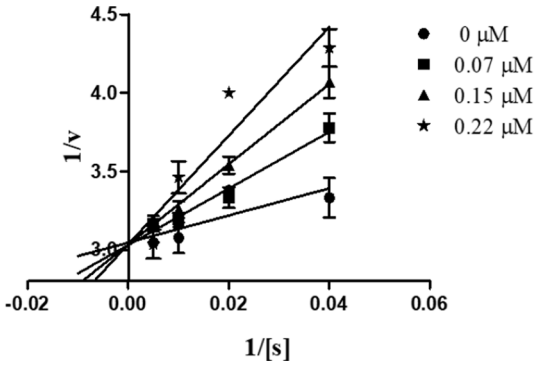

Fig. 2. Mode of inhibition of *h*-NTPDase2 inhibitor (**2d**) indicated by Lineweaver-Burk Plot. Inhibitor (**2d**) was used at following concentrations (μM): 0, 0.07, 0.15 and 0.22.

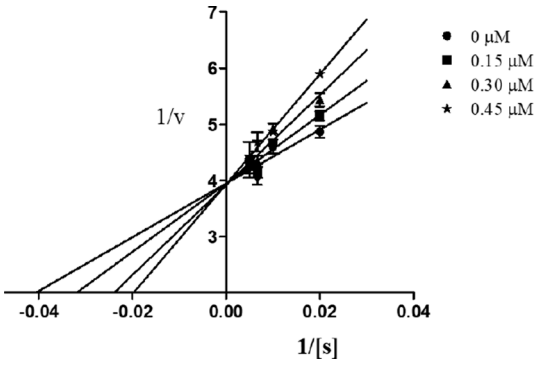

Fig. 3. Mode of inhibition of *h*-NTPDase3 inhibitor (**2a**) indicated by Lineweaver-Burk Plot. Inhibitor (**2a**) was used at following concentrations (μM): 0, 0.15, 0.30 and 0.45.

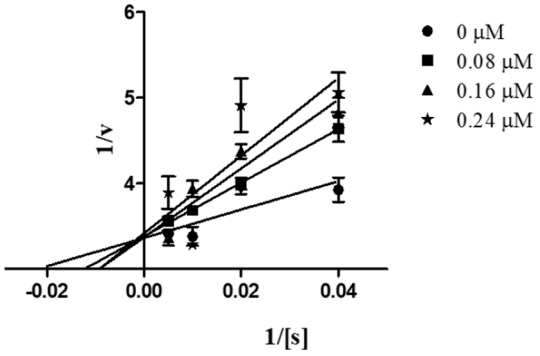

Fig. 4. Mode of inhibition of *h*-NTPDase8 inhibitor (**2a**) indicated by Lineweaver-Burk Plot. Inhibitor (**2a**) was used at following concentrations (μM): 0, 0.08, 0.16 and 0.24.

islets under low and high glucose condition. Negative control (containing no drug) and positive control (containing IBMX) were also included in the study. As shown in Fig. 5, compound **2a** elicited an outstanding surge in insulin release in comparison to control that was 16.7 mM glucose alone. The compound **2a** was evaluated at various concentrations (10 μM to 200 μM); it demonstrated a dose-dependent behavior indicating a maximum effect on insulin secretion at 200 μM (Fig. 6). The compound **2a** had no prominent effect under low glucose concentration since glucose is regarded as the bona fide initiator of insulin secretion, while ATP promotes this insulin secretion in the presence of elevated glucose levels [8].

In contrast, compound **2b** and **2i** did not show any significant

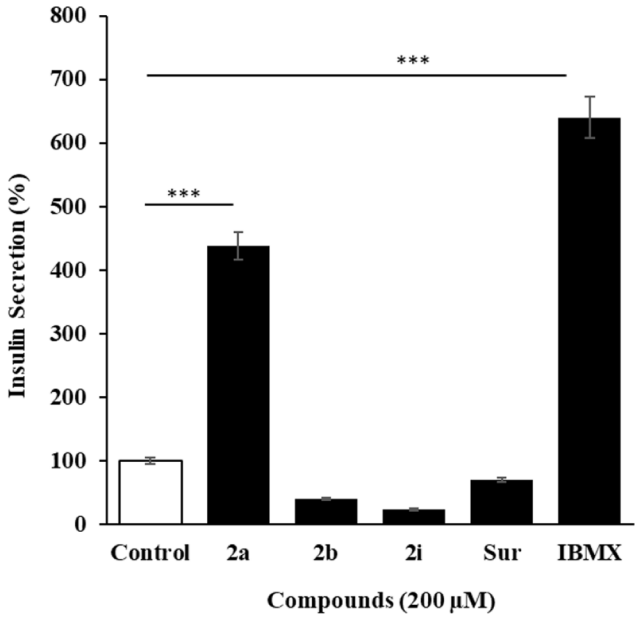

Fig. 5. The effect of compounds **2a, 2b, 2i,** suramin (Sur) and IBMX on insulin secretion in mice islets under stimulation of 16.7 mM glucose. Data are shown as mean ± S.E.M. from 2 to 3 separate experiments. Insulin release resulting from 16.7 mM glucose (alone) was assumed to be 100% and set as control. ***$P < 0.001$ *vs.* none.

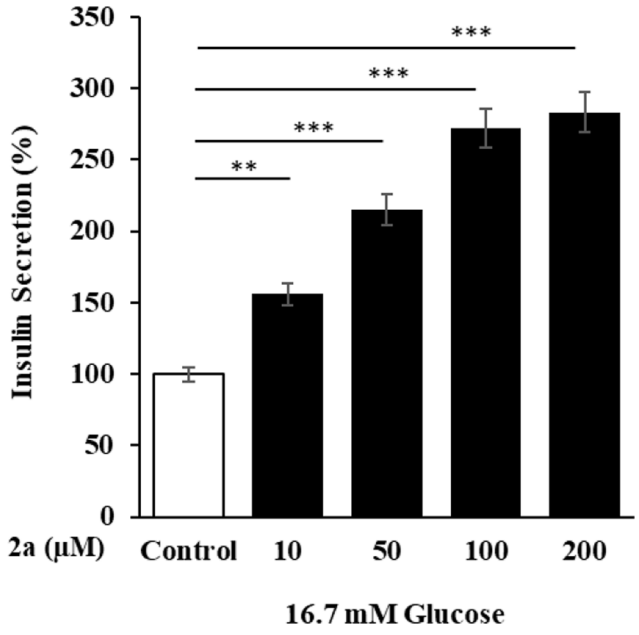

Fig. 6. Effect of different doses of test compound (**2a)** at high glucose concentration (16.7 mM) on insulin secretion. The compound (**2a**) was added at the concentrations of 10 µM, 50 µM, 100 µM and 200 µM. Data are shown as mean ± S.E.M. from 2 to 3 separate experiments. ***$P < 0.001$, **$P < 0.01$.

activity, although both of these compounds showed good activity against *h*-NTPDase3. Suramin, used as positive control throughout enzyme inhibition experiments, also had no significant activity. Thus by blocking the ATP hydrolysis, NTPDase3 inhibitor (**2a**) is participating in the regulation of insulin secretion. Since NTPDase3 has been reported to be the only ectonucleotidase abundantly expressed in pancreatic islets of human and mice, it is the NTPDase3 inhibition that provokes the insulin release. Within this framework, Syed et al., performed a study where they identified the NTPDase3 as the most dominant isoform and

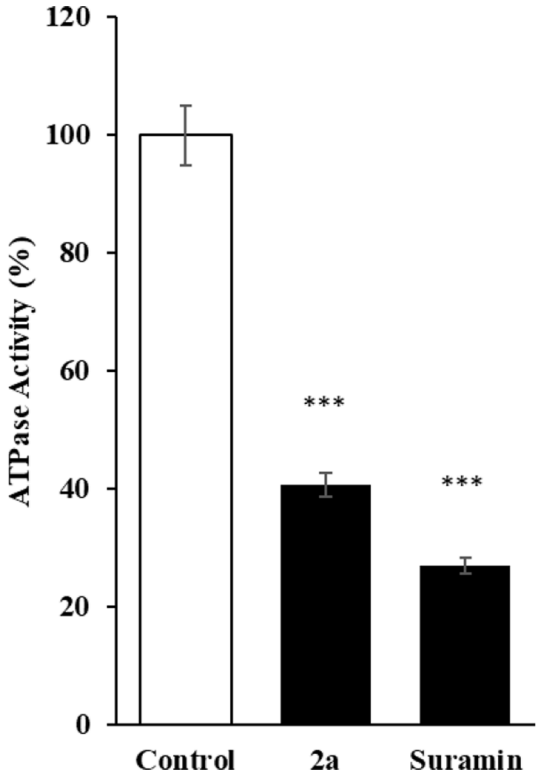

Fig. 7. Test compound **2a** and suramin significantly reduced the ectonucleotidase activity in mice islets' homogenate. A complete enzymatic reaction in the absence of inhibitor was assumed to be 100% and set as control. Data are shown as means ± SEM from three separate experiments. ***$P < 0.0001$.

exploited the ARL67156 as a non-selective inhibitor of NTPDase to establish that it was the suppression of NTPDase3 activity that was culminating itself in the stimulation of insulin release. Moreover, they carried out the siRNA studies to confirm these results [34].

3.4. Effect of compound 2a on ectonucleotidase activity in isolated mice islets

Since compound **2a** appeared to be a potent NTPDase3 inhibitor that was also involed in the modulation of insulin release, we intended to determine how this compound (**2a**) was affecting the ectonucleotidase activity. Hence, freshly isolated islets were transformed into an homogenate which was then incubated with compound **2a** (100 µM) and then malachite green assay was used to establish the ectonucleotidase activity. The results indicated that treating the islets with **2a** substantialy reduced the ectonucleotidase activity and this compound **2a** (in terms of activity) was equivalent to that of suramin (Fig. 7). Subsequently, a concentration–response curve was constructed and compound was observed to reduce the ectonucleotidase activity in a dose-dependent manner (Fig. 8).

3.5. Effect of compound 2a on expression of NTPDase3 mRNA

To further explore the action of compound **2a** on mRNA of NTPDase3, mice pancreatic islets were isolated and treated with compound **2a** for 3 h. Subsequently, total RNA was isolated from these islets and analyzed by quantitative real time PCR. The results indicated that NTPDase3 mRNA level was not significantly affected by NTPDase3 inhibitor (**2a**) exposure. Hence, this inhibition of NTPDase3 did not produced any change at gene level and only inhibition of protein led to regulation of insulin secretion (Fig. 9).

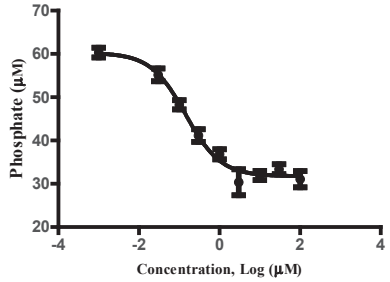

Fig. 8. Different concentrations of compound **2a** inhibited the ectonucleotidase activity (in islets' homogenate) that was measured in the form of Pi liberated from externally introduced ATP (100 μM). Data points indicate the mean ± SEM from three separate experiments.

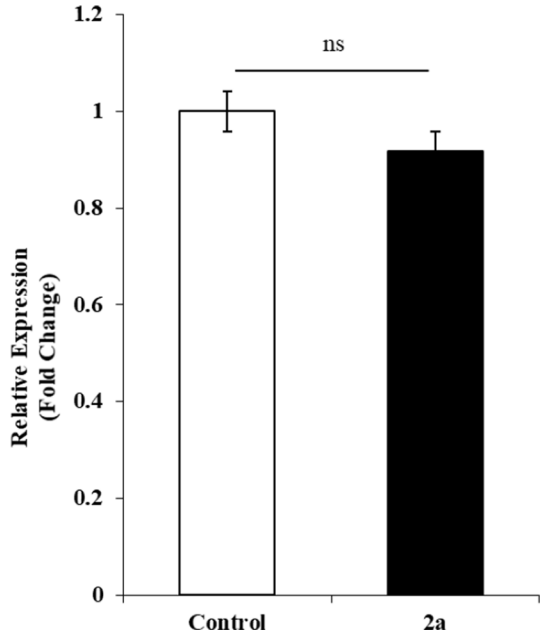

Fig. 9. Effect of compound **2a** on NTPDase3 mRNA by qPCR. The compound **2a** was incubated with islets for 3 h at 37 °C in KRB buffer in the presence of 16.7 mM. RNA was isolated for RT-qPCR. Data was normalized to β-actin. Values are mean ± S.E.M. from 2 to 3 independent experiments. Control, gene expression of the group treated with 16.7 mM glucose only. ns: none significant.

3.6. Molecular docking studies of carboxamide derivatives

In order to determine the putative binding mode, molecular docking studies of the most potent inhibitors were performed for respective isozyme. Considering the mode of inhibition, compounds possessing a competitive mechanism of inhibition were selected for docking studies. Thus compound **2a** and **2d** were docked within the active site of respective enzyme.

While docking the compound **2d** within the active pocket of modelled *h*-NTPDase2, three hydrogen bonds were formed with Arg392 through imine and amide functionalities of the compound. The side chain of Ala393 was involved in pi-alkyl interaction with 4-chloro phenyl ring whereas, indole ring appeared to be stabilized by involving in a pi-pi stacked interaction with Tyr350 and His50 (Fig. 10).

The docking analysis of compound **2a** displayed a number of interactions with different amino acids inside the active pocket of modelled *h*-NTPDase3. As shown in Fig. 11, the indole ring of compound **2a** was making a hydrogen bond with Arg67 through its C═O group. The amine functionality was also involved in hydrogen bond interaction with aromatic side chain of Trp549. Similarly, both NH of amide group

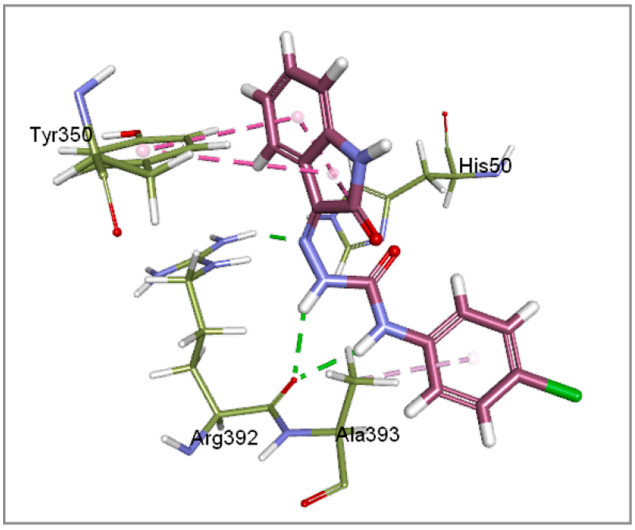

Fig. 10. Three dimensional interaction pose of **2d** docked in human NTPDase2 model.

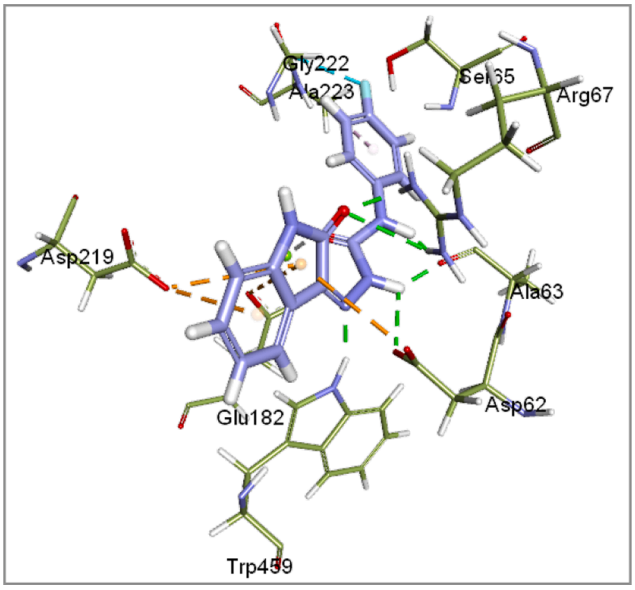

Fig. 11. Three dimensional interaction pose of **2a** docked in human NTPDase3 model.

were making hydrogen bond with Ala63 whereas, another hydrogen bond was formed between NH group and Asp62. The indole ring was experiencing several pi-anion interactions with Asp62, Asp219 and Glu182. Moreover, a pi-alkyl interaction was also noticed between Ala223 and 4-fluoro phenyl ring.

The amino acid residues lining the catalytic site of *h*-NTPDase8 were comprised of His53, Asp48, Tyr59, Gly42, Trp440, Val436, Thr441 and Leu442. The compound was attached to active site via non-covalent bond formation, including hydrogen bond, pi-pi stacking and pi-anion interactions. In this regard, imine group (C═N) was making hydrogen bond with Trp440 and Thr441 whereas, another hydrogen bond was formed between fluorine and His53. Similarly, Asp48 was also observed to have a hydrogen bond interaction with NH of amide functionality. The alkyl groups in Val436 and Leu442 were observed to have pi-alkyl interaction with indole phenyl ring, while Tyr59 was found to be involved in the pi-pi (*T*-shaped) interaction with the same ring (Fig. 12).

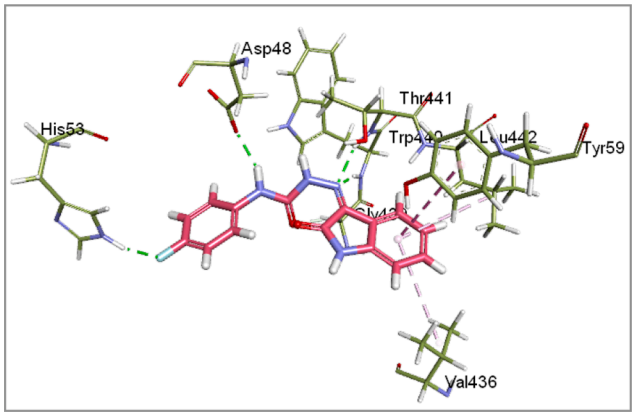

Fig. 12. Three dimensional interaction pose of **2a** docked in human NTPDase8 model.

4. Conclusion

In conclusion, oxoindolin phenylhydrazine carboxamide derivatives (**2a-j**) were synthesized by two step reactions and obtained in good yield. They were tested as inhibitors of *h*-NTPDases, including *h*-NTPDase1, −2, −3 and −8. Most of the compounds exhibited promising activity against *h*-NTPDase1 with IC_{50} values in the low micro-molar range. Interestingly, four compounds (**2e**, **2f**, **2g** and **2h**) were found to be selective inhibitors of *h*-NTPDase1whereas, compound **2b** was identified as selective *h*-NTPDase3 inhibitor. Compound **2a**, **2b** and **2i**, among the potent/selective NTPDase3 inhibitors, were further evaluated to determine their effects on insulin secretion using mice islets. These findings indicated that compound **2a** had strongly influenced the insulin release and it was also involved in the reduction of ectonucleotidase activity in mice islets. Moreover, docking analysis suggested that the binding modes of investigated compounds were in compliance with *in vitro* results. Hence, compound **2a** is anticipated to become a valuable pharmacological tool to further elucidate the role of NTPDase3 in insulin secretion.

Declaration of Competing Interest

The authors declare that they have no known competing financial interests or personal relationships that could have appeared to influence the work reported in this paper.

Acknowledgements

This work was financially supported by the German.

Academic Exchange Service (DAAD) "German-Pakistani Research Collaboration Programme". J.S received support from the Natural Sciences and Engineering Research Council of Canada (RGPIN-2016-05867).

Appendix A. Supplementary material

Supplementary data to this article can be found online at https://doi.org/10.1016/j.bioorg.2021.104957.

References

[1] L. Wei, F. Mousawi, D. Li, S. Roger, J. Li, X. Yang, L.H. Jiang, ATP release and P2 receptor signalling in Piezo1 channel-dependent mechanoregulation, Front. Pharmacol. 10 (2019) 1304, https://doi.org/10.3389/fphar.2019.01304.

[2] L. Dou, Y.F. Chen, P.J. Cowan, X.P. Chen, Extracellular ATP signaling and clinical relevance, Clin. Immunol. 188 (2018) 67–73, https://doi.org/10.1016/j.clim.2017.12.006.

[3] A.L. Giuliani, A.C. Sarti, F.D. Virgilio, Extracellular nucleotides and nucleosides as signalling molecules, Immunol. Lett. 205 (2019) 16–24, https://doi.org/10.1016/j.imlet.2018.11.006.

[4] A. Taruno, ATP release channels, Int. J. Mol. Sci. 19 (2018) 808, https://doi.org/10.3390/ijms19030808.

[5] G. Scarpellino, T. Genova, L. Munaron, Purinergic P2X7 receptor: a cation channel sensitive to tumor microenvironment, Recent Pat. Anti-cancer Drug Discovery 14 (2019) 32–38, https://doi.org/10.2174/1574892814666190116122256.

[6] M. Tozzi, A.T. Larsen, S.C. Lange, A. Giannuzzo, M.N. Andersen, I. Novak, The P2X7 receptor and pannexin-1 are involved in glucose-induced autocrine regulation in β-cells, Sci. Rep. 8 (2018) 8926, https://doi.org/10.1038/s41598-018-27281-9.

[7] M. Vakilian, Y. Tahamtani, K. Ghaedi, A review on insulin trafficking and exocytosis, Gene 706 (2019) 52–61, https://doi.org/10.1016/j.gene.2019.04.063.

[8] M. Cieślak, M. Cieślak, Role of purinergic signalling and proinflammatory cytokines in diabetes, Clin. Diabetol. 6 (2017) 90–100, https://doi.org/10.5603/DK.2017.0015.

[9] J.C. Henquin, Paracrine and autocrine control of insulin secretion in human islets: evidence and pending questions, Am. J. Physiol. Endocrinol. Metab. 320 (2020) E78–E86, https://doi.org/10.1152/ajpendo.00485.2020.

[10] G. Kasuya, Y. Fujiwara, H. Tsukamoto, S. Morinaga, S. Ryu, K. Touhara, R. Ishitani, Y. Furutani, M. Hattori, O. Nureki, Structural insights into the nucleotide base specificity of P2X receptors, Sci. Rep. 7 (2017) 45208, https://doi.org/10.1038/srep45208.

[11] G. Kasuya, T. Yamaura, X.B. Ma, R. Nakamura, M. Takemoto, H. Nagumo, E. Tanaka, N. Dohmae, T. Nakane, Y. Yu, R. Ishitani, Structural insights into the competitive inhibition of the ATP-gated P2X receptor channel, Nat. Commun. 8 (2017) 876, https://doi.org/10.1038/s41467-017-00887-9.

[12] C. Blanchard, E. Boué-Grabot, K. Massé, Comparative embryonic spatio-temporal expression profile map of the Xenopus P2X receptor family, Front. Cell. Neurosci. 13 (2019) 340, https://doi.org/10.3389/fncel.2019.00340.

[13] A. Solini, I. Novak, Role of the P2X7 receptor in the pathogenesis of type 2 diabetes and its microvascular complications, Curr. Opin. Pharmacol. 47 (2019) 75–81, https://doi.org/10.1016/j.coph.2019.02.009.

[14] O.H. Petersen, A. Verkhratsky, Calcium and ATP control multiple vital functions, Phil. Trans. R. Soc. B. 371 (2016) 20150418, https://doi.org/10.1098/rstb.2015.0418.

[15] I.V. Kügelgen, Pharmacology of P2Y receptors, Brain Res. Bull. 151 (2019) 12–24, https://doi.org/10.1016/j.brainresbull.2019.03.010.

[16] R. Lu, Z. Zhang, C. Jiang, Recent progress on the discovery of P2Y14 receptor antagonists, Eur. J. Med. Chem. 175 (2019) 34–39, https://doi.org/10.1098/rstb.2015.0418.

[17] C. Bartley, T. Brun, L. Oberhauser, M. Grimaldi, F. Molica, B.R. Kwak, D. Bosco, M. Chanson, P. Maechler, Chronic fructose renders pancreatic β-cells hyperresponsive to glucose-stimulated insulin secretion through extracellular ATP signaling, Am. J. Physiol. Endocrinol. Metab. 317 (2019) E25–E41, https://doi.org/10.1152/ajpendo.00456.2018.

[18] S.Y. Lee, S. Sarkar, S. Bhattarai, V. Namasivayam, S.D. Jonghe, H. Stephan, P. Herdewijn, A. El-Tayeb, C.E. Müller, Substrate-dependence of competitive nucleotide pyrophosphatase/phosphodiesterase1 (NPP1) inhibitors, Front. Pharmacol. 8 (2017) 54, https://doi.org/10.3389/fphar.2017.00054.

[19] S.Y. Lee, C.E. Müller, Nucleotide pyrophosphatase/phosphodiesterase 1 (NPP1) and its inhibitors, MedChemComm. 8 (2017) 823–840, https://doi.org/10.1039/C7MD00015D.

[20] M. Tozzi, I. Novak, Purinergic receptors in adipose tissue as potential targets in metabolic disorders, Front. Pharmacol. 8 (2017) 878, https://doi.org/10.3389/fphar.2017.00878.

[21] I. Grković, D. Drakulić, J. Martinović, N. Mitrović, Role of Ectonucleotidases in Synapse Formation During Brain Development: Physiological and Pathological Implications, Curr. Neuropharmacol. 17 (2019) 84–98, https://doi.org/10.2174/1570159X15666170518151541.

[22] D.D. Nabinger, S. Altenhofen, C.D. Bonan, Zebrafish models: Gaining insight into purinergic signaling and neurological disorders, Prog. Neurosychopharmacol. Biol. Psychiatry 98 (2020), https://doi.org/10.1016/j.pnpbp.2019.109770.

[23] M.S. Longhi, A. Moss, Z.G. Jiang, S.C. Robson, Purinergic signaling during intestinal inflammation, J. Mol. Med. 95 (2017) 915–925, https://doi.org/10.1007/s00109-017-1545-1.

[24] L. Schäkel, C.C. Schmies, R.M. Idris, X. Luo, S.Y. Lee, V. Lopez, S. Mirza, J. Pelletier, J. Sevigny, V. Namasivayam, C.E. Müller, Nucleotide analog ARL67156 as a lead structure for the development of CD39 and dual CD39/CD73 ectonucleotidase inhibitors, Front. Pharmacol. 11 (2020) 1294, https://doi.org/10.3389/fphar.2020.01294.

[25] M.D. Bagatini, A.A. dos Santos, A.M. Cardoso, A. Mânica, C.R. Reschke, F. B. Carvalho, The impact of purinergic system enzymes on noncommunicable, neurological, and degenerative diseases, J. Immunol. Res. 2018 (2018) 4892473, https://doi.org/10.1155/2018/4892473.

[26] B. Allard, M.S. Longhi, S.C. Robson, J. Stagg, The ectonucleotidases CD 39 and CD 73: novel checkpoint inhibitor targets, Immunol. Rev. 276 (2017) 121–144, https://doi.org/10.1111/imr.12528.

[27] A.H. Zhong, Z.G. Jiang, R.D. Cummings, S.C. Robson, Various N-glycoforms differentially upregulate E-NTPDase activity of the NTPDase3/CD39L3 ectoenzymatic domain, Purinergic Signal. 13 (2017) 601–609, https://doi.org/10.1007/s11302-017-9587-y.

[28] L.G. Castilhos, S.A. Adefegha, P.H. Doleski, T.M.D. Bertoldo, C.E.J. Moritz, E. A. Casali, D.B.R. Leal, NTPDase, 5′-nucleotidase and adenosine deaminase

activities and purine levels in serum of sickle cell anemia patients, J. App. Biomed. 16 (2018) 208–213, https://doi.org/10.1016/j.jab.2017.12.004.
[29] A.P.S. Bertoni, R.P. de Campos, A.S.K. Tamajusuku, G.P. Stefani, E. Braganhol, A. M.O. Battastini, M.R. Wink, Biochemical analysis of ectonucleotidases on primary rat vascular smooth muscle cells and in silico investigation of their role in vascular diseases, Life Sci. 256 (2020), https://doi.org/10.1016/j.lfs.2020.117862.
[30] L. Paes-Vieira, A.L. Gomes-Vieira, J.R. Meyer-Fernandes, NTPDase activities: possible roles on Leishmania spp infectivity and virulence, Cell Biol. Int. 42 (2018) 670–682, https://doi.org/10.1002/cbin.10944.
[31] D.C. Saunders, M. Brissova, N. Phillips, S. Shrestha, J.T. Walker, R. Aramandla, G. Poffenberger, D.K. Flaherty, K.P. Weller, J. Pelletier, T. Cooper, M.T. Goff, J. Virostko, A. Shostak, E.D. Dean, D.L. Greiner, L.D. Shultz, N. Prasad, S.E. Levy, R.H. Carnahan, C. Dai, J. Sévigny, A.C. Powers, Ectonucleoside triphosphate diphosphohydrolase-3 antibody targets adult human pancreatic β cells for in vitro and in vivo analysis, Cell Metab. 29 (2019) 745–754, https://doi.org/10.1016/j.cmet.2018.10.007.
[32] E.G. Lavoie, M. Fausther, G. Kauffenstein, F. Kukulski, B.M. Künzli, H. Friess, J. Sévigny, Identification of the ectonucleotidases expressed in mouse, rat, and human Langerhans islets: potential role of NTPDase3 in insulin secretion, Am. J. Physiol. Endocrinol. Metab. 299 (2010) E647–E656, https://doi.org/10.1152/ajpendo.00126.2010.
[33] S.K. Syed, A.L. Kauffman, L.S. Beavers, J.T. Alston, T.B. Farb, J. Ficorilli, M. C. Marcelo, M.B. Brenner, K. Bokvist, D.G. Barrett, A.M. Efanov, Ectonucleotidase NTPDase3 is abundant in pancreatic β-cells and regulates glucose-induced insulin secretion, Am. J. Physiol. Endocrinol. Metab. 305 (2013) E1319–E1326, https://doi.org/10.1152/ajpendo.00328.2013.
[34] S.A. Levesque, É.G. Lavoie, J. Lecka, F. Bigonnesse, J. Sévigny, Specificity of the ecto-ATPase inhibitor ARL 67156 on human and mouse ectonucleotidases, Br. J. Pharmacol. 152 (2007) 141–150, https://doi.org/10.1038/sj.bjp.0707361.
[35] J. Lecka, M. Fausther, B. Künzli, J. Sévigny, Ticlopidine in its prodrug form is a selective inhibitor of human NTPDase1, Mediators Inflamm. 2014 (2014), https://doi.org/10.1155/2014/547480.
[36] M.M. Bradford, A rapid and sensitive method for the quantitation of microgram quantities of protein utilizing the principle of protein-dye binding, Anal. Biochem. 72 (1976) 248–254, https://doi.org/10.1016/0003-2697(76)90527-3.
[37] M. Martín-Satué, E.G. Lavoie, J. Pelletier, M. Fausther, E. Csizmadia, O. Guckelberger, S.C. Robson, J. Sévigny, Localization of plasma membrane bound NTPDases in the murine reproductive tract, Histochem. Cell. Biol. 131 (2009) 615–628, https://doi.org/10.1007/s00418-008-0551-3.
[38] A. Hameed, R.M. Hafizur, N. Hussain, S.A. Raza, M. Rehman, S. Ashraf, Z. Ul-Haq, F. Khan, M.I. Choudhary, Eriodictyol stimulates insulin secretion through cAMP/PKA signaling pathway in mice islets, Eur. J. Pharmacol. 820 (2018) 245–255, https://doi.org/10.1016/j.ejphar.2017.12.015.
[39] C.J. Hedeskov, K. Capito, The effect of starvation on insulin secretion and glucose metabolism in mouse pancreatic islets, Biochem. J. 140 (1974) 423–433, https://doi.org/10.1042/bj1400423.
[40] J. Iqbal, S.J.A. Shah, Molecular dynamic simulations reveal structural insights into substrate and inhibitor binding modes and functionality of Ecto-Nucleoside Triphosphate Diphosphohydrolases, Sci. Rep. 8 (2018) 1–11, https://doi.org/10.1038/s41598-018-20971-4.
[41] LeadIT, 2014, at http://www.biosolveit.de/LeadIT/.